science.sciencemag.org/content/366/6466/714/suppl/DC1

Supplementary Material for

Direct observation of changing NO_x lifetime in North American cities

Joshua L. Laughner and Ronald C. Cohen*

*Corresponding author. Email: rccohen@berkeley.edu

Published 8 November 2019, *Science* **366**, 714 (2019)
DOI: 10.1126/science.aax6832

This PDF file includes:

Materials and Methods

The BErkeley High Resolution NO_2 Product

We use version 3.0B with daily NO_2 profiles of the BErkeley High Resolution (BEHR) NO_2 Product, described in detail in (*12*) and validated in (*25*). Briefly, the BEHR product is based on the NASA OMI NO_2 Standard Product, version 3.0 (*26*), but with custom tropospheric air mass factors (AMFs). These AMFs are calculated using higher resolution surface reflectance (MODIS MCD43D BRDF product, (*27–30*)), terrain elevation (GLOBE topographic database, (*31*)), and NO_2 a priori profiles (simulated at daily, 12 km resolution). Although the product with daily NO_2 *a priori* profiles limits the analysis to 2005–2014, we have previously shown that these profiles are necessary to get optimum results for NO_x lifetimes (*14*).

Selection of cities for the study

The 49 cities selected for this study were based on the list given in (*32*), Table A1. These cities were shown by that study to be indicative of NO_x trends in North America. Of the 47 cities listed therein, Vancouver, BC had to be removed because it fell outside the BEHR v3.0B domain. Three additional cities were added: Austin, TX and Baltimore, MD as large urban areas not included in the Russell at al. study, and Cheyenne, WY was added as it contains the NCAR-Wyoming Supercomputing Center. Of these 49, 12 had zero or one valid fits given the criteria described under "Lifetime quality filtering" below and therefore could not be used. 3 had valid fits but no statistically significant trend. Of the remaining 34, 3 had lifetime trend shapes more complex than the four simple groups could capture and 3 only had two good quality fits (Fig. S1, also see "Lifetime quality filtering" below).

Line density calculation and fitting

NO_2 line densities and lifetimes are calculated similarly to (*8*) and (*18*). For each day in the observation time period, the wind direction over each location is calculated as the average of winds over the first five layers of a 3 × 3 set of 12 km WRF-Chem grid boxes centered on that location. The WRF-Chem model is that used in (*12*); a North American domain of 405 × 254 grid boxes at with 29 levels centered on 97º W, 39º N was used. Meteorological initial and boundary conditions were taken from the North American Regional Reanalysis (NARR) (*33*). U and V winds, temperature, and water vapor were nudged every 3 hours for all levels with nudging coefficients of 0.0003 s^{-1}. The distance downwind, upwind, and perpendicular to the wind direction included in the line densities are defined by boxes manually chosen for each city to minimize the influence of other nearby sources while still capturing the full plume (see "Effect of box size", below). Some wind directions were also excluded due to overlap with other nearby sources (Table S3).

BEHR NO_2 columns from each day were rotated so that the wind directions were aligned. Only days with an average wind speed > 3 m s^{-1} are used. A time average of the rotated columns, weighted by the inverse of the pixel area is computed, and then integrated in the across-wind direction to produce a line density. NO_2 columns with cloud fraction 0.2, viewing zenith angle >60º, or flagged as in the row anomaly (http://projects.knmi.nl/omi/research/product/rowanomaly-background.php) are not included. These line densities are fit with an exponentially-modified Gaussian (EMG) function (*10*, *18*):

$$F(x \mid a, x_0, \mu_x, \sigma_x, B) = \frac{a}{2x_0} \exp\left(\frac{\mu_x}{x_0} + \frac{\sigma_x^2}{2x_0^2} - \frac{x}{x_0}\right) \operatorname{erfc}\left(-\frac{1}{\sqrt{2}}\left[\frac{x-\mu_x}{\sigma_x} - \frac{\sigma_x}{x_0}\right]\right) + B \qquad \text{(S1)}$$

where a, x_0, μ_x, σ_x, and B are fitting parameters. We use a non-linear interior point minimization algorithm (fmincon in Matlab) to minimize the cost function:

$$R(a, x_0, \mu_x, \sigma_x, B) = \sum_x \left(F(x \mid a, x_0, \mu_x, \sigma_x, B) - \mathrm{NO_2}(x) \right)^2 \quad \text{(S2)}$$

where F is the EMG fitting function from and $\mathrm{NO_2}(x)$ the line densities. To avoid unphysical results, constraints are placed on the fitting parameters (Table S1). The rationale for these constraints is the same as in (*14*).

The fitting procedure is repeated 10 times for each line density. For the first attempt a best guess of the initial values for the five fitting parameters is used (Table S2). For the remaining 9 attempts, random values are used. The fit with the smallest residual by is kept as the best fit. The entire process is repeated twice for each city, and if the best fits do not agree, that fit is discarded.

Lifetime calculation

The fitting parameter x_0 is related to the plume average $\mathrm{NO_x}$ lifetime by:

$$\tau = \frac{x_0}{w} \quad \text{(S3)}$$

where w is the average wind speed for that location.

The absolute uncertainty of the lifetime is calculated as:

$$\sigma_\tau = \tau \left[\left(\frac{\sigma_{x_0}}{x_0} \right)^2 + \left(\frac{\sigma_{\mathrm{VCD}}}{\sqrt{n}} \right)^2 + \sigma_b^2 + \sigma_w^2 \right]^{1/2} \quad \text{(S4)}$$

where

- σ_{x_0} is the uncertainty in the x_0 parameter
- σ_{VCD} is the uncertainty in the NO_2 vertical column densities (25%)
- n is the number of observations used in calculating the line densities. It is computed as the minimum number of pixels that contribute to the time average of any one grid cell during the line density calculation.
- σ_b is the uncertainty due to across wind integration distance (10%)
- σ_w is the uncertainty due to the choice of wind fields (30%)

These uncertainties are assigned based on (*10*) and (*18*). The uncertainty in x_0 is computed as a 95% confidence interval for $m - 5$ degrees of freedom, where m is the number of points in the line density. The standard deviation needed for the confidence interval is calculated as:

$$\sigma_i = \frac{R(a, x_0, \mu_x, \sigma_x, B)}{m-5} h_i^{-1} \tag{S5}$$

where R is the residual from Eq. (S2) and h_i^{-1} is the ith diagonal element on the inverse Hessian matrix returned by the minimization at the final solution (*34*).

However, when considering trends, this error is likely an overestimate of the relative error between years for the same location, as part of the errors will be correlated across years:

- Errors in polluted VCDs are largely attributable to the air mass factor (AMF). Errors in the AMF are in turn attributable to its inputs: surface reflectance, surface pressure, and

NO_2 profile shape. Biases in any of these can persist across years even if day-specific inputs are used if the models representing them are unable to adequately represent the true state around the city.

- The effect on lifetime due to box width was shown by (*10*) to monotonically increase with box width; since we use the same box width for all years, this error should be entirely correlated.
- Unresolved complexity in terrain can lead to systematic errors in wind fields (*35*). Therefore, at least part of the error due to wind fields is likely correlated.

The temporal correlation of these errors is not well studied. However, Beirle et al. (*10*) computed the standard mean error (SME) in the fit among line densities along wind directions divided into 8 sectors, and found that this error was 10% to 40%. Since the 8 sectors used to calculate the SME are for the same city, their variation is a reasonable representation of the uncorrelated error to expect in a trend. Therefore, 10% is likely the lower bound for uncorrelated error in these trends. However, since we cannot explicitly separate the correlated and uncorrelated error in the lifetime trends, we retain the absolute lifetime error calculated as above as a conservative value when testing for significance of the trends.

To test whether any two lifetimes are statistically different, we use a two sample t-test. Since the lifetimes have different uncertainties, we use the form (*36*):

$$t_{\text{calc}} = \frac{|\tau_1 - \tau_2|}{\sqrt{\frac{\sigma_1^2}{n_1} + \frac{\sigma_2^2}{n_2}}} \tag{S6}$$

$$n_{\mathrm{DoF}} = \frac{\left(\sigma_1^2 / n_1 + \sigma_2^2 / n_2\right)^2}{\frac{(\sigma_1^2 / n_1)^2}{n_1 - 1} + \frac{(\sigma_2^2 / n_2)^2}{n_2 - 1}} \quad \text{(S7)}$$

and consider the difference statistically significant if $t_{\mathrm{calc}} > t(95\%, n_{\mathrm{DoF}})$ for a two-sided *t*-test. Here, τ is the lifetime, σ the standard deviation calculated by propagating the value for x_0 from Eq. (S5) with Eq. (S4) and n is the number of points in the line densities. We tested reducing n by 5 to be the number of degrees of freedom of each lifetime as a conservative check; it did not affect our results.

Lifetime quality filtering

Visual examination of any selection of line densities and fits demonstrates that the fitting is not always able to reproduce the observed shape of the line densities, therefore criteria to identify accurate vs. inaccurate fits were required. To avoid biasing the results, four criteria were developed by simulating idealized line densities with fixed first-order lifetimes, identifying under which circumstances the fitting failed, and refining the criteria until they successfully accept good fits and reject bad fits.

In detail, we generated line densities from an ideal 2D multibox model (*37*) with a constant emission source and a prescribed first order lifetime. The model simulated a 2D Gaussian NO source with a total emission of 17.78 Mg NO h^{-1} (based off emissions of Chicago, IL) with a wind speed of 5 m s^{-1} in the *x*-direction and diffusion coefficients of 100 m^2 s^{-1} in both *x* and *y* directions. The NO_x lifetime in the model was represented as a fixed first-order loss. For model lifetimes between 1 and 9 h and emission widths between 3 and 162 km the model was run to steady state and the resulting 2D plume integrated perpendicular to the wind to generate a

modeled line density. These line densities (with a small amount of random noise, ±5%) were fit and the fitted lifetime compared to the specified lifetime for that run. If the fitted and model lifetimes were within 10%, that fit was considered correct, otherwise it was considered incorrect.

We tested various criteria to classify the fits as good or bad by testing whether the criteria correctly identified fits with the lifetime within 10% of the modeled lifetime as good (true positive) and outside 10% as bad (true negative) or incorrectly classified fits within 10% as bad (false negative) or outside 10% as good (false positive). We found that the following 4 criteria correctly accepted or rejected all but one fit when the line density had 61 data points:

1. $R^2 > 0.8$

2. At least 1.5 lifetimes downwind of the plume center are within the domain

3. The mean of the EMG fit is not different from the mean of the line density for any window of 20 points (test for systematic bias, see Fig. S4b). For every possible window of 20 adjacent points in the line density and fit, the means are computed and tested if they are statistically different. If so, this indicates that the fit lies systematically above or below the line density and that this fit should be rejected as the lifetime will be biased.

4. $\sigma_x < x_0$. This checks that the emission width is not greater than the lifetime distance, which would potentially cause the emission shape to confound the lifetime.

We also tested how the number of points in the line density affects the accuracy of the quality criteria (Fig. S5), varying the number of points used from 31 to 136. We found that the lowest fraction of times the quality filters incorrectly identified the fit as good (false positives) or bad (false negatives) requires 60-90 points in the line density. However, line densities with as few as

46 points are still well characterized by the quality filtering, and since the majority of our line densities have 46–60 points, we did not apply any quality filtering based on the number of points.

Another source of error in the NO_2 lifetime could be the upper limit imposed by vertical mixing and other non-chemical lifetimes. As NO_x from the boundary layer mixes into the free troposphere, wind shear can act as an additional pseudo-loss process. (*38*) estimated the effective lifetime due to vertical mixing to be ~10 h. Similarly, (*18*) note that the lifetimes derived from the EMG fitting are effective lifetimes that include effects such as plume meandering and grid resolution. Assuming these non-chemical lifetimes are reasonably constant over the study period, the effect on the trends will be to underestimate the year-to-year differences in chemical lifetime: since lifetimes add inversely (i.e. $\tau_{total} = [1/\tau_1 + 1/\tau_2 + \ldots + 1/\tau_n]^{-1}$), these non-chemical lifetimes will place an upper limit equal to their value on the observed lifetime. As the chemical lifetime increases, the observed lifetime will asymptotically approach the inverse sum of the non-chemical lifetimes, increasing more slowly than it would if the chemical lifetime alone was observed. The effect of vertical mixing is likely to be small in this study, since nearly all the observed lifetimes were < 5 hr, but the magnitude of the other non-chemical lifetimes has not been quantified. Because these non-chemical lifetimes decrease the observed lifetime relative to the chemical lifetime, but do not change the derivative with respect to NO_x, the only effect on this study should be to underestimate the actual change of chemical lifetimes. Therefore, any change deemed significant given the observed change will also represent a significant change in the chemical lifetime.

Finally, as we see in Fig. S1b, the lifetime in San Francisco is much longer than any of the other cities investigated (~6 h). This is likely because San Francisco is situated on a peninsula that is

much longer in the north-south direction than east-west. This means the emission source is not Gaussian, and so the lifetime fitting may be attributing part of the emission shape to the lifetime. We tested removing San Francisco from our analysis; doing so does not change our conclusions. Since it passes the above quality filtering, we elected to leave it in the analysis.

Effect of box size

Beirle et al. (*10*) found that the box length and width alter the fitted lifetime by 5% and 10% respectively in tests done on the Riyadh, Saudi Arabia plume. Riyadh is much more isolated than many of the cities investigated in this study. However, our selection of box sizes aimed to limit the interference of nearby sources, making the source patterns we analyzed effectively as isolated as Riyadh. This was necessary to ensure accurate fitting, and implies that the effects of box length and width on the fitted lifetime found by (*10*) are applicate to this work.

We have also tested the box length using modeled line densities. The results described above fitting various numbers of points (31 to 136) in the line densities from the 2D box model also demonstrate that, even if fitting too many or too few points adversely affects the lifetime, the quality criteria determined above are generally successful at removing that fit from consideration. Therefore, we believe that the specific choice of box length does not affect the trends found in this work. In general, we chose the largest box (up to 2° downwind, 1° left/right/upwind) possible without encountering secondary sources (Fig. S4a) in order to provide as much data as possible for the fit to work with.

Impact of *a priori* data and comparison with other satellite products

Producing NO_2 vertical column densities requires certain *a priori* information, including cloud fraction and height, surface albedo and height, and the vertical distribution of NO_2 in a given

satellite pixel. The subproduct of BEHR v3.0B used in this study (*13*) makes use of NO_2 profiles simulated with WRF-Chem specifically for each retrieved day, including trends in emissions of various species.

In order to check that the lifetime trends found in this work were not overly influenced by these modeled *a priori* profiles, we fit lifetimes to line densities calculated directly from WRF-Chem. Of the 29 cities that had good quality fits in both the BEHR and WRF-Chem, 18 (62%) fell into different categories (increasing, decreasing, CCU, CCD, complex, or no trend) in BEHR vs. WRF-Chem. This indicates that it is unlikely that the lifetimes obtained from the BEHR line densities are simply mirroring the lifetime imposed in WRF-Chem.

Similarly, we fit lifetimes to line densities computed from the NASA Standard Product 3 (SP3, (*26*, *39*)). Of the 33 cities with good fits from both NASA and BEHR line densities, 19 (58%) fell into different categories. In (*14*), we had found that the lifetime was similar between a retrieval using spatially coarse, monthly average *a priori* profiles (as SP3 does) and one using spatially fine, daily *a priori* profiles (as BEHR does). We suspect that the difference in results is simply due to the larger sample here, finding cases where the coarse *a priori* profiles do affect the results. This could happen if the border between two 1° grid cells that the NASA *a priori* profiles are simulated in occurs partway along the line density and causes a sharp drop or increase in the line density. In theory, the BEHR retrieval should provide a better representation of the line densities, as the *a priori* profiles are at the same resolution as the OMI pixels and account for the day-to-day variations in wind speed/direction.

Steady-state model

The steady state model used to generate Fig. 1 and Fig. S6 is conceptually similar to that in (*40*) except that OH, HO_2, and RO_2 are solved for separately. The model assumes that HO_2, RO_2, and the whole HO_x family are each individually in steady state considering the reactions:

$$RO_2 + NO \xrightarrow{1-\alpha} RO + NO_2 \longrightarrow HO_2 \quad \text{R1}$$
$$RO_2 + NO \xrightarrow{\alpha} RONO_2 \quad \text{R2}$$
$$HO_2 + NO \longrightarrow NO_2 + OH \quad \text{R3}$$
$$HO_2 + HO_2 \longrightarrow HOOH + O_2 \quad \text{R4}$$
$$RO_2 + HO_2 \longrightarrow ROOH + O_2 \quad \text{R5}$$
$$RH + OH \longrightarrow RO_2 \quad \text{R6}$$
$$RO_2 + R'O_2 \longrightarrow ROOR' + O_2 \quad \text{R7}$$
$$NO_2 + OH \longrightarrow HNO_3 \quad \text{R8}$$

We then write the following set of equations:

$$[HO_2] = \frac{(1-\alpha)k_{RO_2+NO}[RO_2][NO]}{k_{HO_2+NO}[NO] + 2k_{HO_2+HO_2}[HO_2] + k_{RO_2+HO_2}[RO_2]} \quad \text{(S8)}$$

$$[RO_2] = \frac{VOC_R[OH]}{k_{RO_2+NO}[NO] + k_{RO_2+HO_2}[HO_2] + 2k_{RO_2+RO_2}[RO_2]} \quad \text{(S9)}$$

$$P(HO_x) = k_{OH+NO_2}[OH][NO_2] + \alpha k_{RO_2+NO}[RO_2][NO] + 2k_{RO_2+HO_2}[RO_2][HO_2] + 2k_{RO_2+RO_2}[RO_2]^2 + 2k_{HO_2+HO_2}[HO_2]^2 \quad \text{(S10)}$$

These equations are solved numerically using "vpasolve" in Matlab. Initial guesses for [HO], $[HO_2]$, and $[RO_2]$ are given by:

$$[OH] = \frac{-b + \sqrt{b^2 - 4ac}}{2a} \quad \text{(S11)}$$

where

$$a = 6k_{5,\text{eff}}\left[\frac{\text{VOC}_\text{R}}{k_{2,\text{eff}}[\text{NO}]}\right]^2$$
$$b = k_4[\text{NO}_2] + \alpha \cdot \text{VOC}_\text{R}$$
$$c = -P(\text{HO}_\text{x})$$

and

$$[\text{RO}_2]_\text{init} = [\text{HO}_2]_\text{init} = \frac{[\text{OH}]_\text{init} \cdot \text{VOC}_\text{R}}{k_{\text{RO}_2+\text{NO}}[\text{NO}]} \quad \text{(S12)}$$

$[NO_x]$, VOC_R, $P(HO_x)$, and α are inputs into the mode. The values for the various rate expressions and other constants are given in Table S5.

MOVES emissions

The MOtor Vehicle Emission Simulator (MOVES) was obtained from https://www.epa.gov/moves/latest-version-motor-vehicle-emission-simulator-moves. To calculate bottom-up NO_x emissions for the required cities, the county at the geographic center of the city was selected, and NO_x emissions from all sources were aggregated to monthly totals.

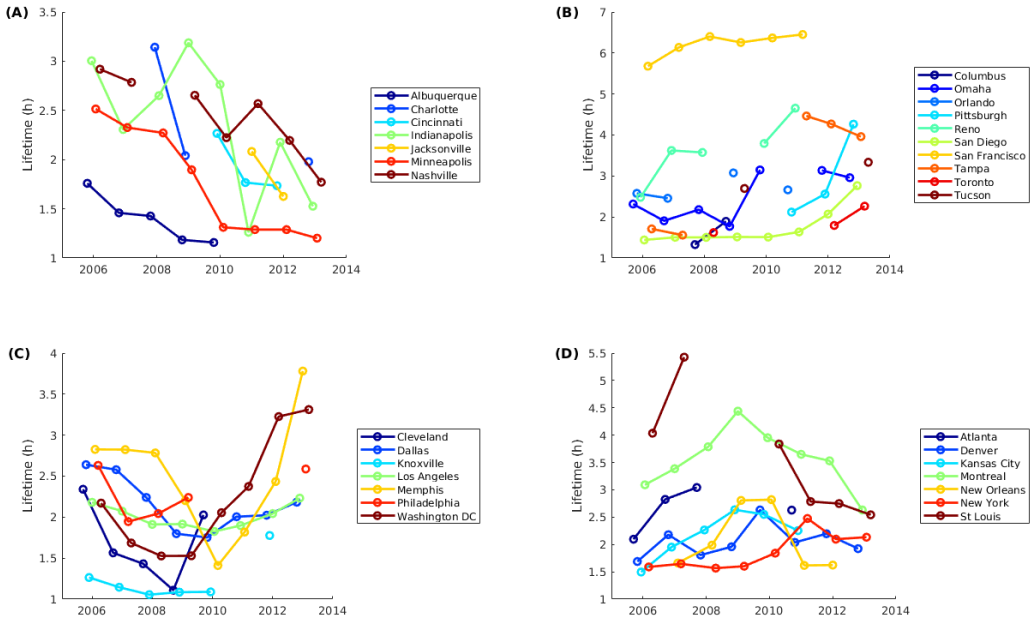

Fig. S1.

Absolute weekday lifetimes in each of the four groups from Fig. 1 of the main paper. Missing years are due to either to the algorithm failing to fit the line density successfully, or from failing the quality criteria discussed above.

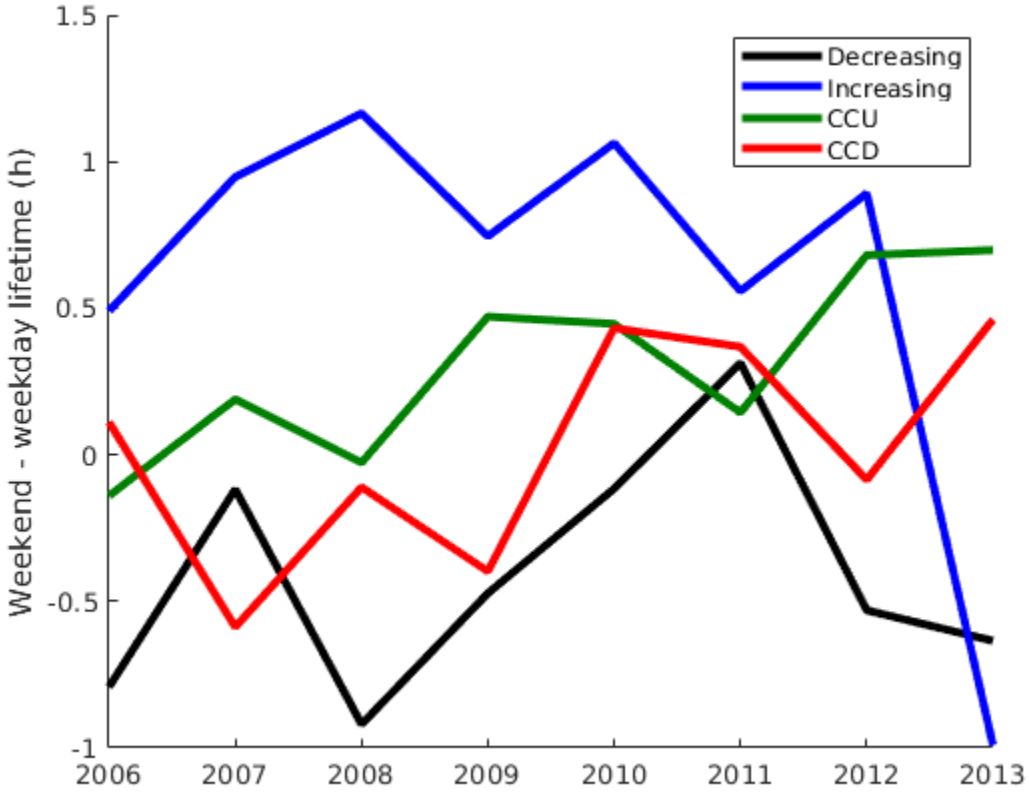

Fig. S2.

Median differences in weekend (Saturday-Sunday) and weekday (Tuesday-Friday) lifetime for each of the four groups of cities in Fig. 3 of the main paper.

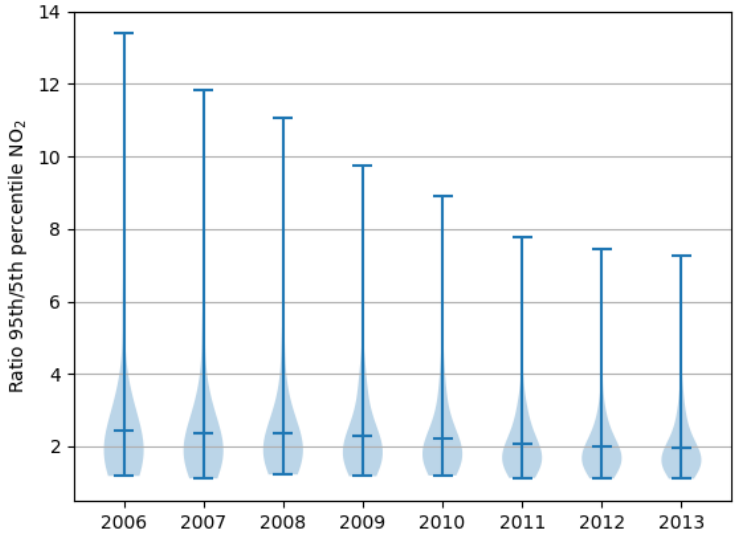

Fig. S3.

Violin plots of the ratio of the 95th percentile of NO_2 line densities to the 5th percentile of line densities upwind of the position of the 95th percentile. Smaller values indicate increasing contribution of the background NO_2 VCDs to the urban average. The top and bottom horizontal lines represent the minimum and maximum of the ratio; the middle horizontal line is the mean. The lighter background shapes' widths are proportional to the number of cities with the corresponding ratio on the y-axis.

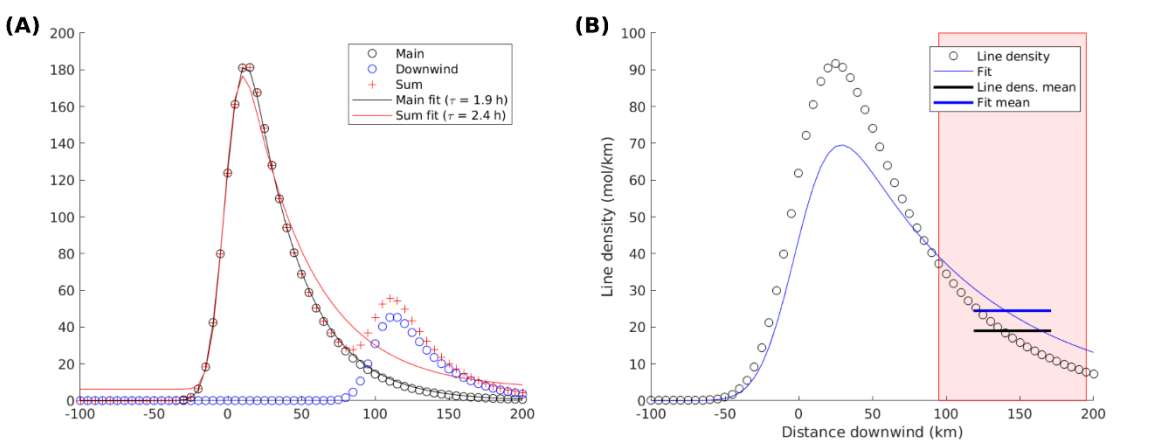

Fig S4.

Hypothetical line densities (circles) and fits (lines) used to demonstrate (a) the problem with downwind sources and (b) the systematic bias test. (a) The sum (red) of a primary source (black) and secondary, downwind source (blue) create a shape not well captured by the EMG function. As a result, the fit of the combined line density (red) decays slower than the true fit of the primary source alone (black) in order to include the secondary source in the fit. (b) The window (red box) is 20 line density points wide, and the thick horizontal lines represent the mean of the line density and fit within that window. If the means are statistically different, the fit is rejected due to probable systematic bias between the fit and line density; here, you can see that the fit may be overestimating the lifetime as it lies above the line density throughout the window. All possible 20 point windows are tested and the fit rejected if any of them have a systematic difference.

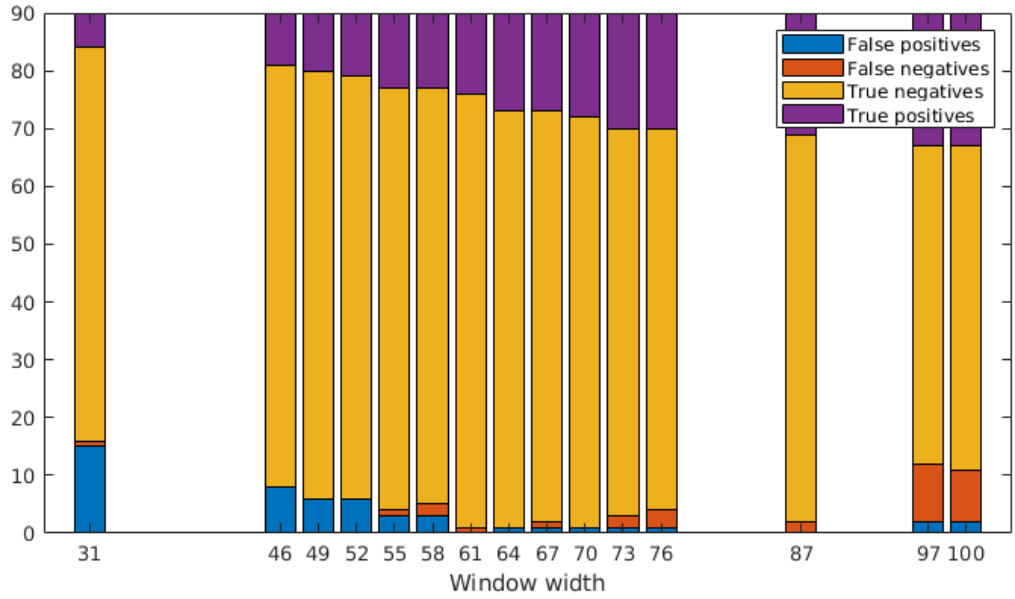

Fig. S5

Effect of the number of points in the line density on the accuracy of the four lifetime fit goodness criteria. “Positive” means the fit is considered good.

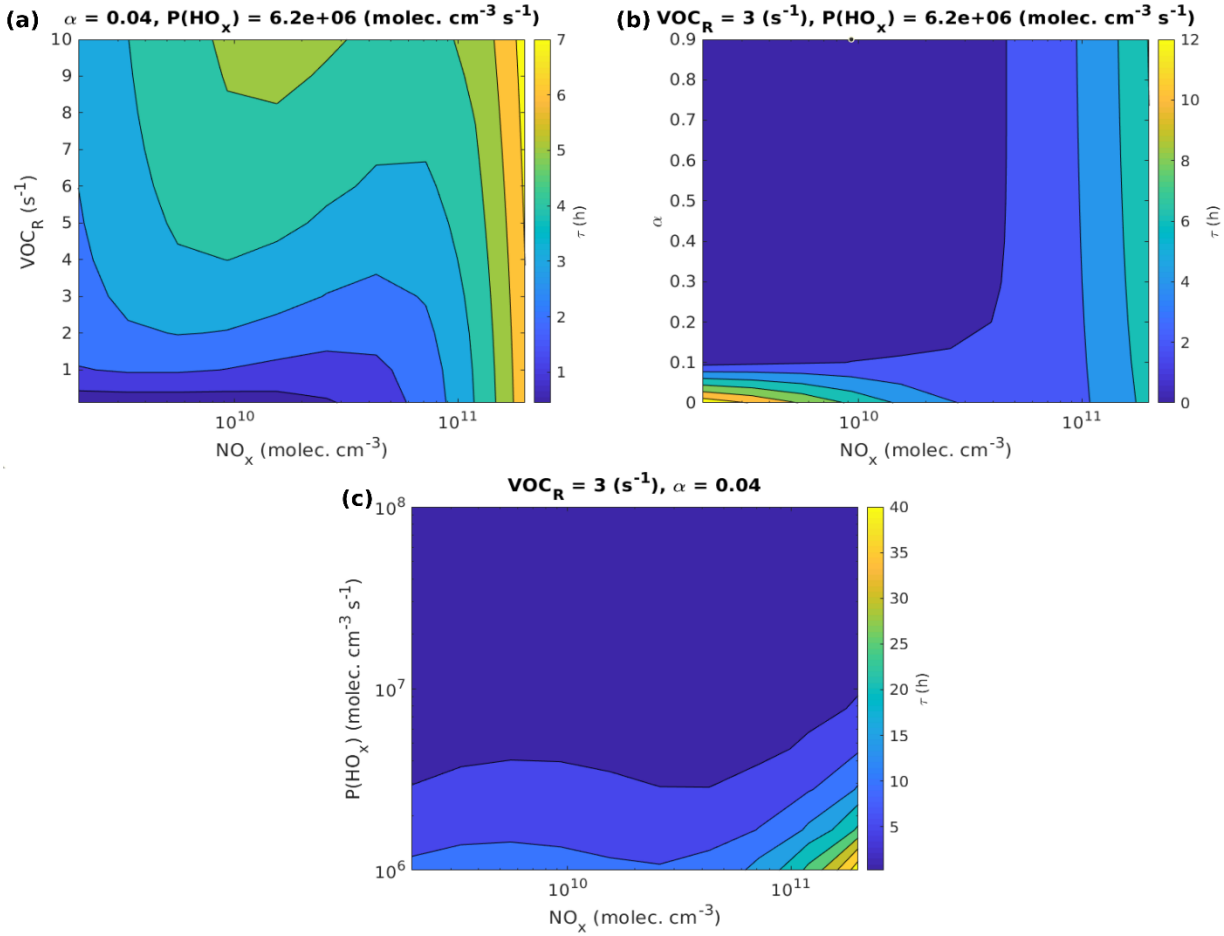

Fig S6

Isopleths of NO_x lifetime vs. NO_x concentration and (a) volatile organic compound OH reactivity (VOC_R), (b) RO_2 + NO alkyl nitrate branching ratio, α, and (c) production of HO_x calculated from the steady state model described above.

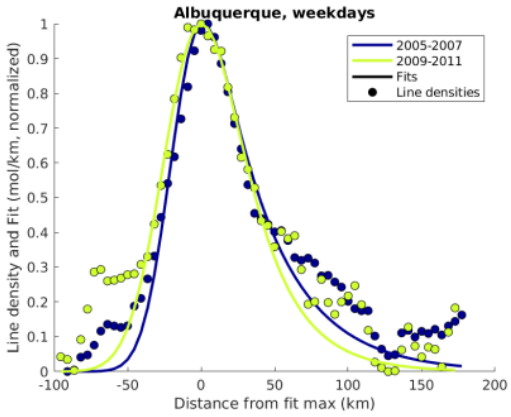
Albuquerque, weekdays
2005-2007
2009-2011
Fits
Line densities
Line density and Fit (mol/km, normalized)
Distance from fit max (km)

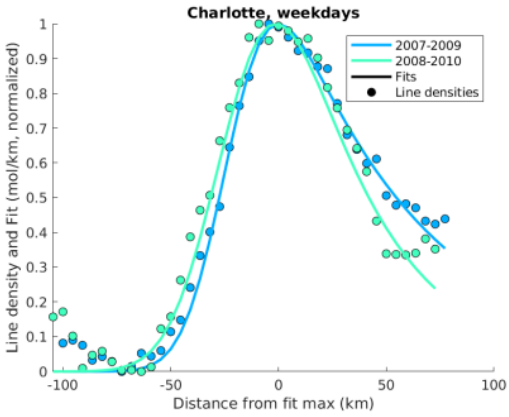
Charlotte, weekdays
2007-2009
2008-2010
Fits
Line densities
Line density and Fit (mol/km, normalized)
Distance from fit max (km)

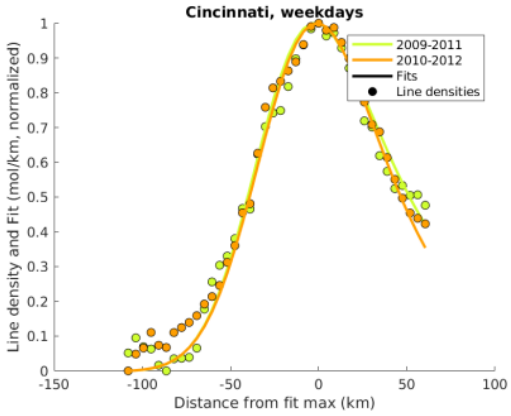
Cincinnati, weekdays
2009-2011
2010-2012
Fits
Line densities
Line density and Fit (mol/km, normalized)
Distance from fit max (km)

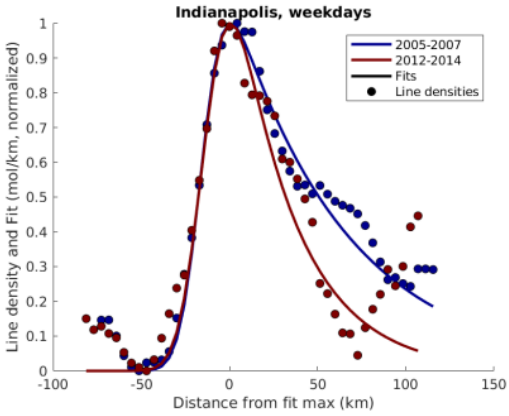
Indianapolis, weekdays
2005-2007
2012-2014
Fits
Line densities
Line density and Fit (mol/km, normalized)
Distance from fit max (km)

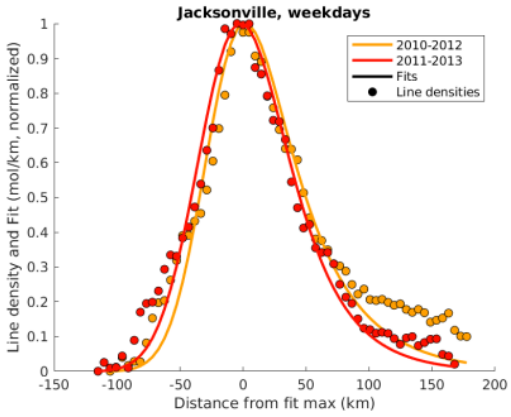
Jacksonville, weekdays
2010-2012
2011-2013
Fits
Line densities
Line density and Fit (mol/km, normalized)
Distance from fit max (km)

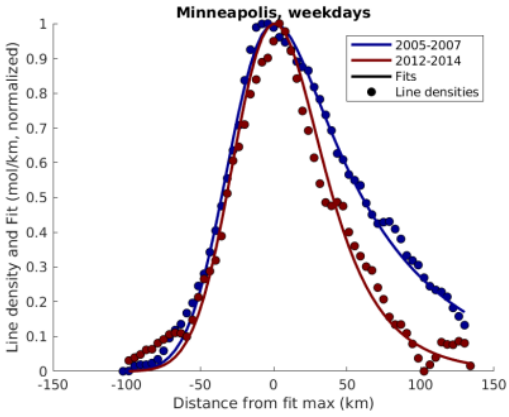
Minneapolis, weekdays
2005-2007
2012-2014
Fits
Line densities
Line density and Fit (mol/km, normalized)
Distance from fit max (km)

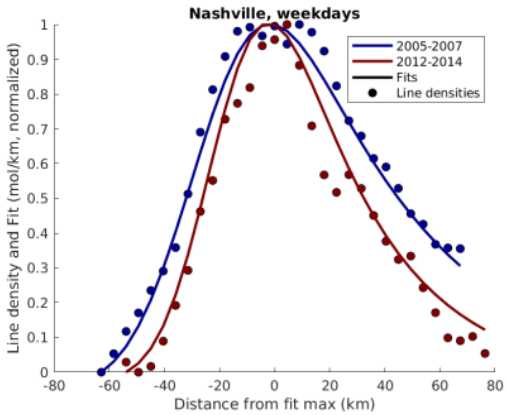
Nashville, weekdays
2005-2007
2012-2014
Fits
Line densities
Line density and Fit (mol/km, normalized)
Distance from fit max (km)

Fig. S7

Line densities and fits for key years of the decreasing lifetime group.

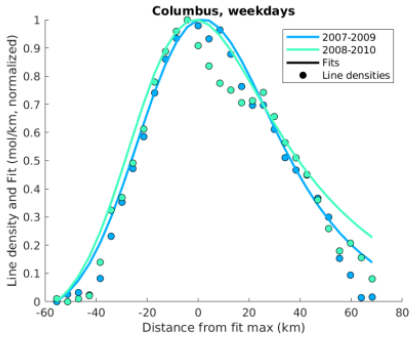
Columbus, weekdays
2007-2009
2008-2010
Fits
Line densities
Line density and Fit (mol/km, normalized)
Distance from fit max (km)

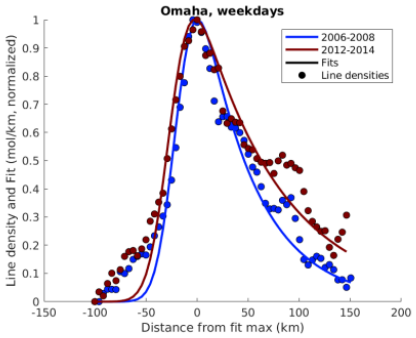
Omaha, weekdays
2006-2008
2012-2014
Fits
Line densities
Line density and Fit (mol/km, normalized)
Distance from fit max (km)

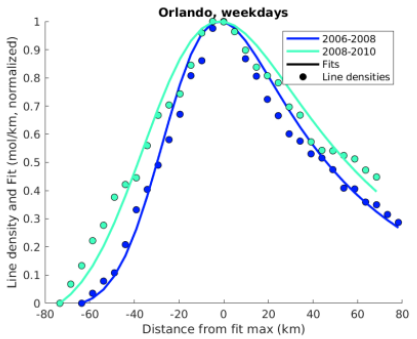
Orlando, weekdays
2006-2008
2008-2010
Fits
Line densities
Line density and Fit (mol/km, normalized)
Distance from fit max (km)

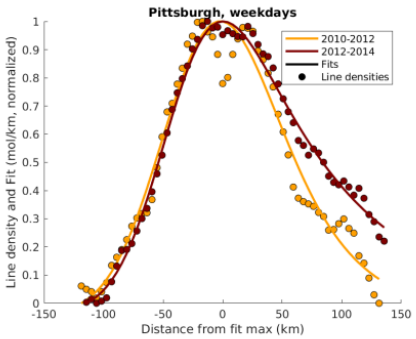
Pittsburgh, weekdays
2010-2012
2012-2014
Fits
Line densities
Line density and Fit (mol/km, normalized)
Distance from fit max (km)

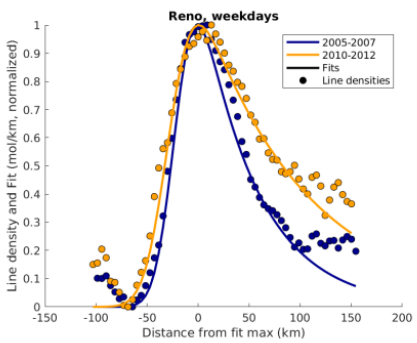
Reno, weekdays
2005-2007
2010-2012
Fits
Line densities
Line density and Fit (mol/km, normalized)
Distance from fit max (km)

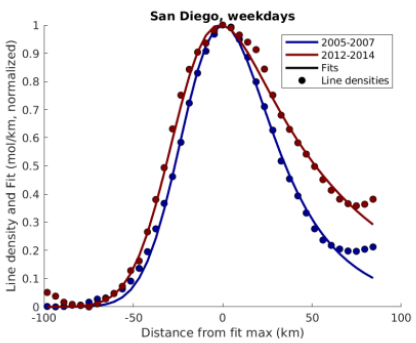
San Diego, weekdays
2005-2007
2012-2014
Fits
Line densities
Line density and Fit (mol/km, normalized)
Distance from fit max (km)

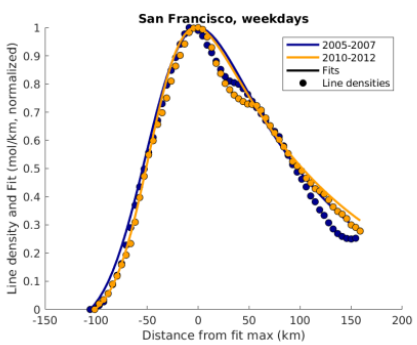
San Francisco, weekdays
2005-2007
2010-2012
Fits
Line densities
Line density and Fit (mol/km, normalized)
Distance from fit max (km)

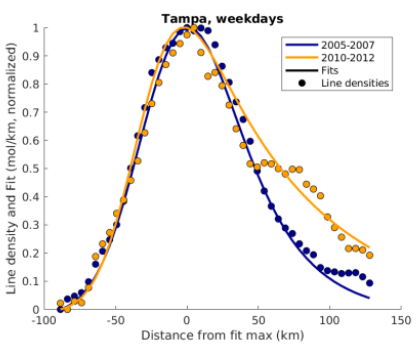
Tampa, weekdays
2005-2007
2010-2012
Fits
Line densities
Line density and Fit (mol/km, normalized)
Distance from fit max (km)

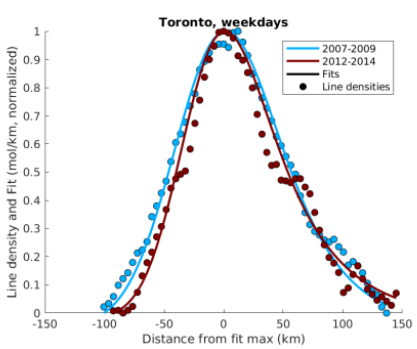
Toronto, weekdays
2007-2009
2012-2014
Fits
Line densities
Line density and Fit (mol/km, normalized)
Distance from fit max (km)

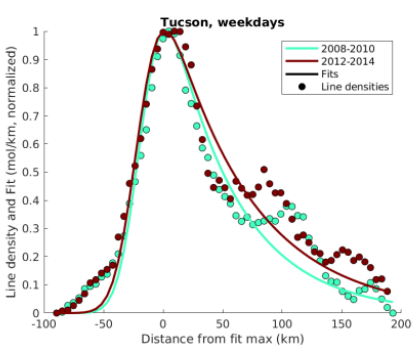
Tucson, weekdays
2008-2010
2012-2014
Fits
Line densities
Line density and Fit (mol/km, normalized)
Distance from fit max (km)

Fig. S8

Line densities and fits for key years for cities in the increasing lifetime group.

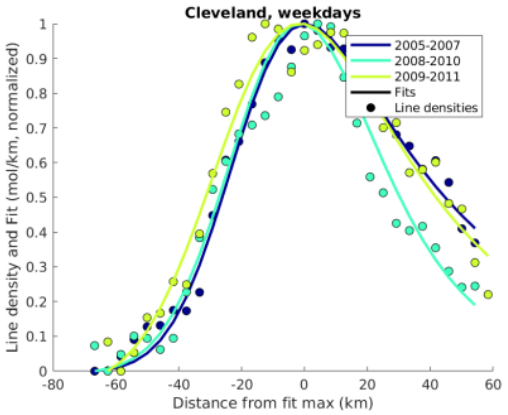
Cleveland, weekdays
2005-2007
2008-2010
2009-2011
Fits
Line densities
Line density and Fit (mol/km, normalized)
Distance from fit max (km)

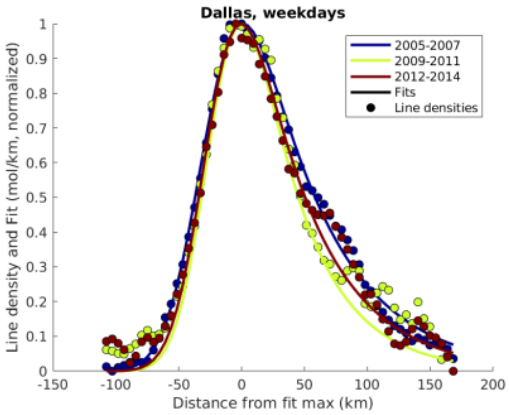
Dallas, weekdays
2005-2007
2009-2011
2012-2014
Fits
Line densities
Line density and Fit (mol/km, normalized)
Distance from fit max (km)

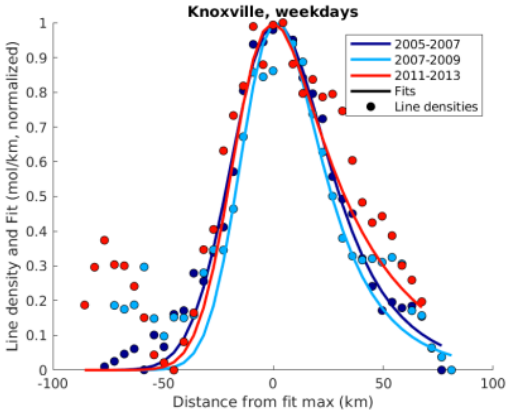
Knoxville, weekdays
2005-2007
2007-2009
2011-2013
Fits
Line densities
Line density and Fit (mol/km, normalized)
Distance from fit max (km)

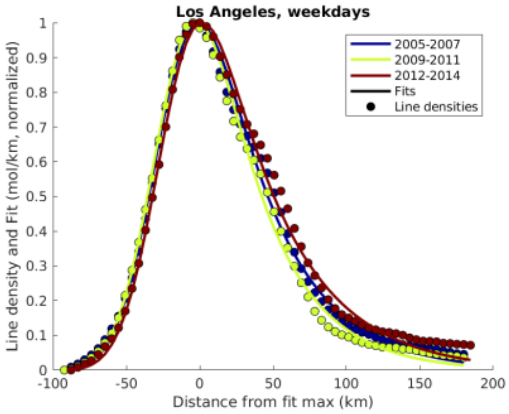
Los Angeles, weekdays
2005-2007
2009-2011
2012-2014
Fits
Line densities
Line density and Fit (mol/km, normalized)
Distance from fit max (km)

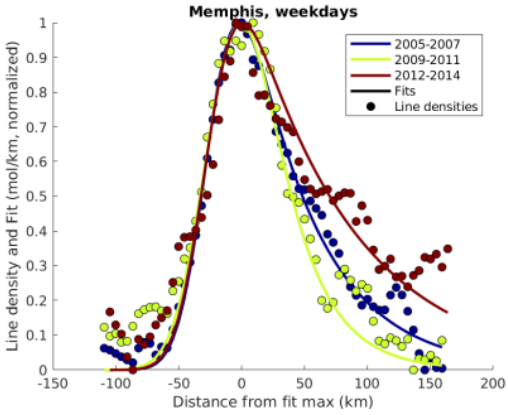
Memphis, weekdays
2005-2007
2009-2011
2012-2014
Fits
Line densities
Line density and Fit (mol/km, normalized)
Distance from fit max (km)

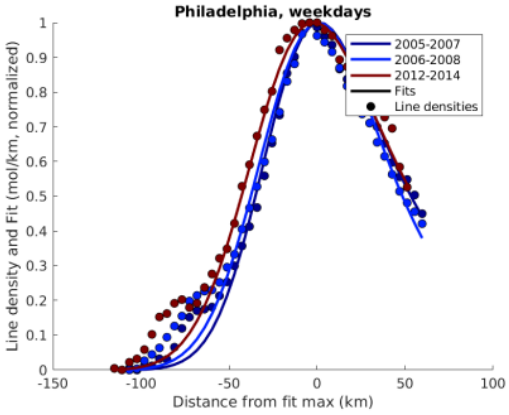
Philadelphia, weekdays
2005-2007
2006-2008
2012-2014
Fits
Line densities
Line density and Fit (mol/km, normalized)
Distance from fit max (km)

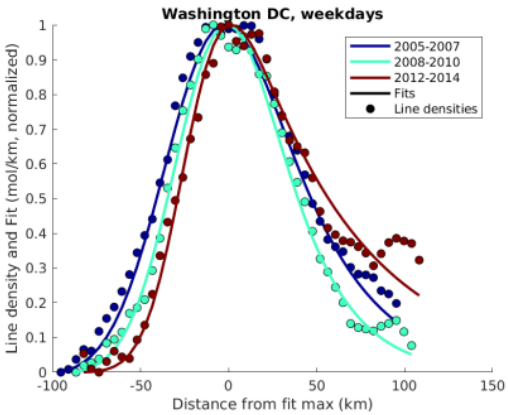
Washington DC, weekdays
2005-2007
2008-2010
2012-2014
Fits
Line densities
Line density and Fit (mol/km, normalized)
Distance from fit max (km)

Fig. S9

Line densities and fits for key years for cities in the concave up (CCU) lifetime group.

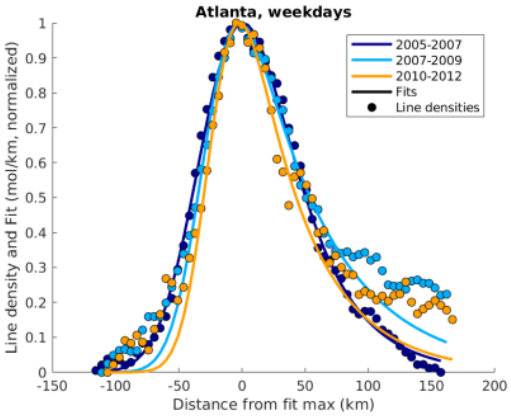
Atlanta, weekdays
2005-2007
2007-2009
2010-2012
Fits
Line densities
Line density and Fit (mol/km, normalized)
Distance from fit max (km)

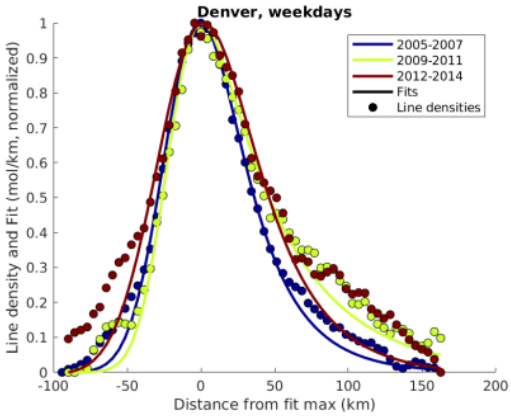
Denver, weekdays
2005-2007
2009-2011
2012-2014
Fits
Line densities
Line density and Fit (mol/km, normalized)
Distance from fit max (km)

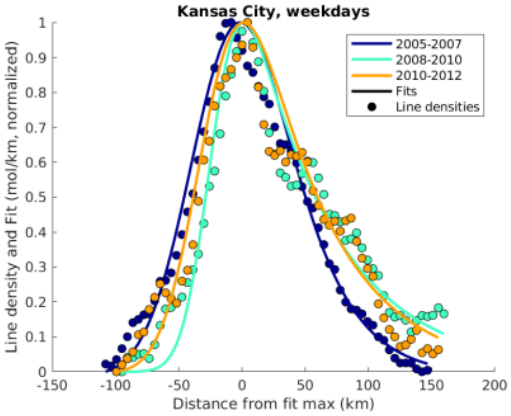
Kansas City, weekdays
2005-2007
2008-2010
2010-2012
Fits
Line densities
Line density and Fit (mol/km, normalized)
Distance from fit max (km)

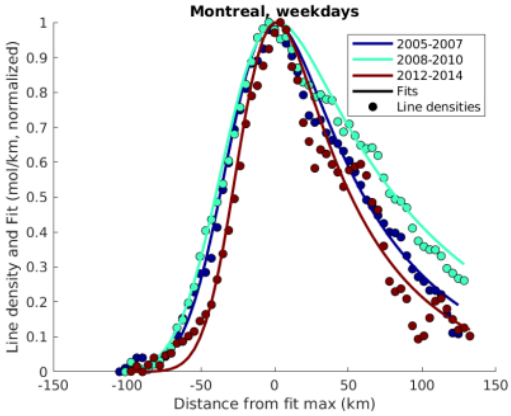
Montreal, weekdays
2005-2007
2008-2010
2012-2014
Fits
Line densities
Line density and Fit (mol/km, normalized)
Distance from fit max (km)

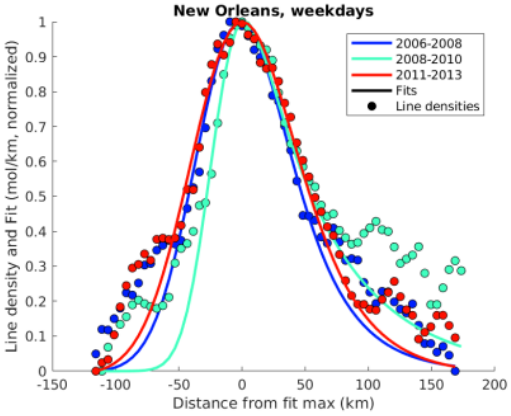
New Orleans, weekdays
2006-2008
2008-2010
2011-2013
Fits
Line densities
Line density and Fit (mol/km, normalized)
Distance from fit max (km)

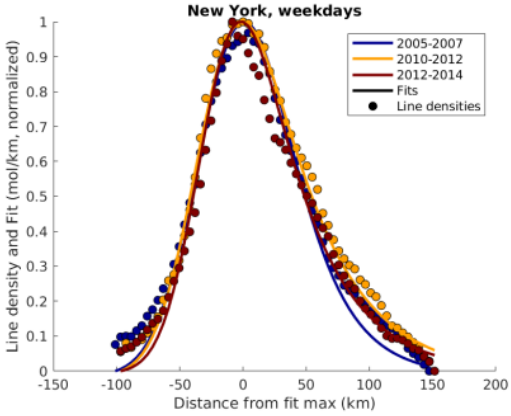
New York, weekdays
2005-2007
2010-2012
2012-2014
Fits
Line densities
Line density and Fit (mol/km, normalized)
Distance from fit max (km)

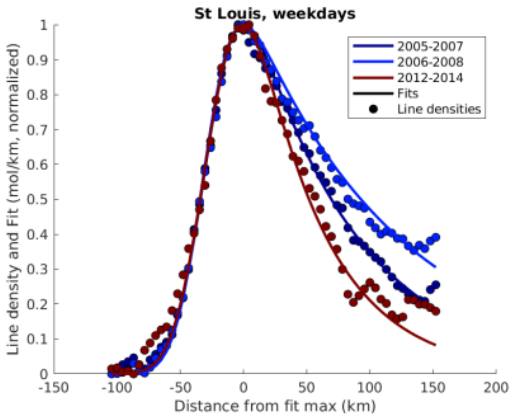
St Louis, weekdays
2005-2007
2006-2008
2012-2014
Fits
Line densities
Line density and Fit (mol/km, normalized)
Distance from fit max (km)

Fig. S10

Line densities and fits for key years for the cities in the concave down (CCD) lifetime group.

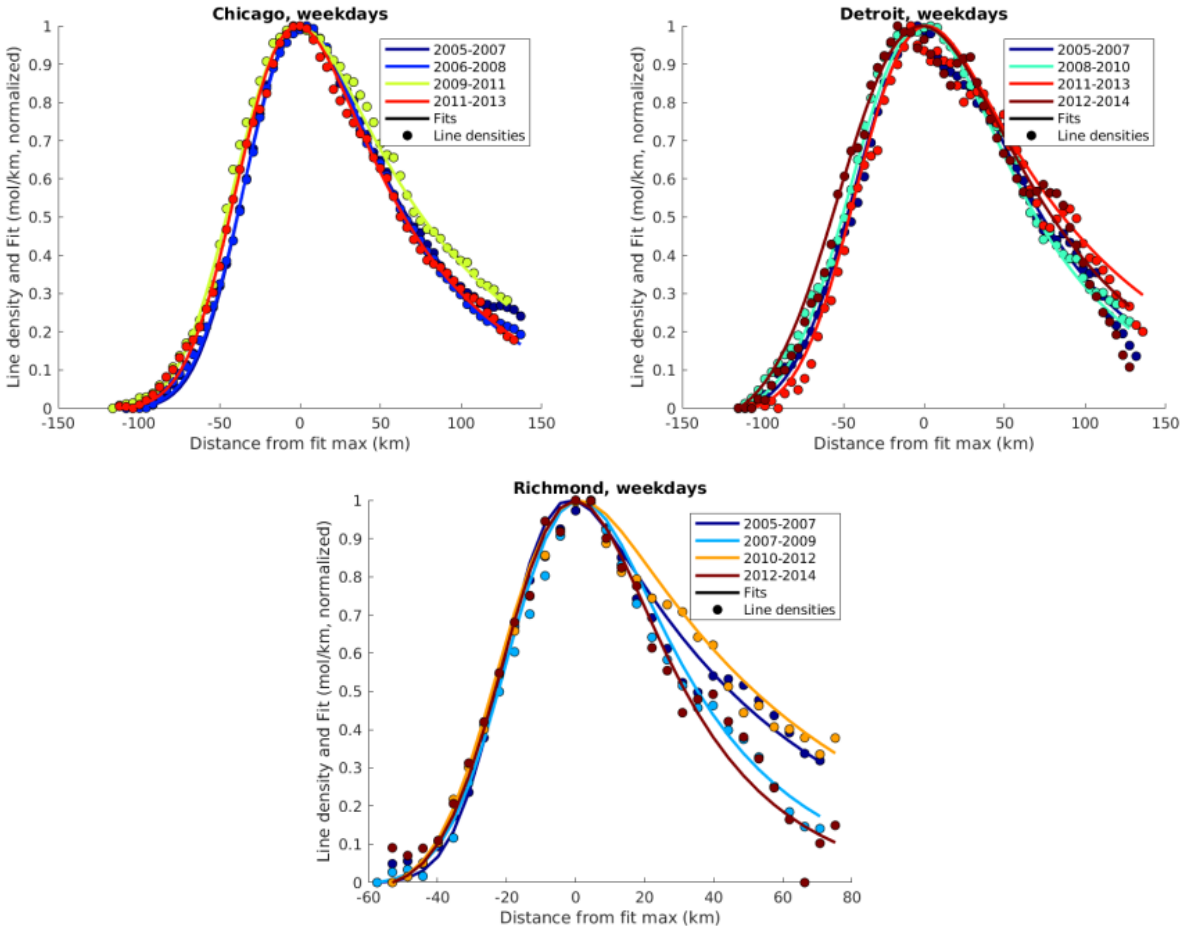

Fig. S11

Line densities and fits for key years for cities that do not fit the in previous four groups.

Table S1.

Constraints imposed on the EMG fitting.

Parameter	Allowed range	Rationale
a	$[0,\infty)$ mol	a represents plume mass, must be positive
x_0	$[1.6,\infty)$ km	$1/e$ distance for exponential, 1.6 km is 1/3 grid spacing. Minimum distinguishable e-folding distance
μ_x	$\mu_x \in x$ km	μ represents plume center, must lie within domain
σ_x	$[\min(x), x(\max(\mathrm{NO_2}))]$	σ represents Gaussian width, assume 3 points required to define a Gaussian, min width at half max is half of 5 km grid cell.
B	$[0, \max(\mathrm{NO_2})]$ mol km^{-1}	B represents background, must be positive and less than maximum line density
Additional constraints		**Rationale**
$\mu_x + x_0 < \max(x)$		At least one lifetime must occur between plume center and edge of domain to be reliably measured
$\exp\left(\frac{\mu_x}{x_0} + \frac{\sigma_x^2}{2x_0^2} - \frac{x}{x_0}\right) < 20$		Prevent the exponential term from approaching infinity in the fitting procedure

Table S2.

Best guesses for initial values of each fitting parameter.

Parameter	Init. value	Rationale
a	$\int_x \mathrm{NO_2}(x)dx$	Since a relates to plume mass, the total line density integral is a reasonable first guess
x_0	54 km	Assuming a 5 m s^{-1} wind and 3 h lifetime to get the e-folding lifetime
μ_x	$x(\max(\mathrm{NO_2}))$	The peak center should be near the maximum line density
σ_x	FWHM/2.355	Estimate the full width-half max of the Gaussian which is 2.355 of its σ
B	$\min(\mathrm{NO_2})$	The minimum line density is a reasonable guess for the background

Table S3

The centers and box widths used to calculate line densities for the cities used in this study. The latitude and longitude give the center coordinates of the city, and the box width describes the size of the box within which line densities are calculated. For example, a box width of [1 2 0.5 0.5] means that NO_2 VCDs 1 degree upwind, 2 degrees downwind, and 0.5 degrees to either side of the center latitude and longitude were used to calculate the line densities. The rejected wind directions column lists wind directions not included in the line densities. The directions specify a 45º cone centered on that direction that the wind is blowing towards. For example, defining an eastward wind direction as 0º, E in this column means any day that the wind vector is between ±22.5º is not included in the line density.

Location	Latitude	Longitude	Box Size (upwind, downwind, left, right) in degrees	Rejected Wind Directions
Albuquerque, NM	35.2	-106.55	[1 2 0.5 0.5]	NW
Atlanta, GA	33.8	-84.35	[1 2 1 1]	SE, E
Austin, TX	30.26	-97.74	[1 2 1 1]	SW
Bakersfield, CA	35.3	-119	[0.5 1 0.5 0.5]	
Baltimore, MD	39.3	-76.2	[1 2 1 1]	NE, SW
Boston, MA	42.45	-71	[1 2 1 1]	S, SW
Charlotte, NC	35.25	-80.85	[1 1 1 1]	
Cheyenne, WY	41.1	-104.8	[1 2 1 1]	
Chicago, IL	41.8	-87.7	[1 2 1 1]	
Cincinnati, OH	39.1	-84.55	[1 1 1 1]	
Cleveland, OH	41.45	-81.67	[0.5 1 1 1]	W
Columbus, OH	40	-83.1	[0.5 1 0.5 0.5]	
Dallas, TX	32.85	-96.95	[1 2 1 1]	
Denver, CO	39.75	-105	[1 2 1 1]	
Detroit, MI	42.35	-83.1	[1 2 1 1]	S
Fresno, CA	36.7	-119.75	[1 2 0.5 0.5]	NW, W, SW, S
Houston, TX	29.8	-95.25	[1 2 1 1]	NE
Indianapolis, IN	39.8	-86.15	[0.75 1.5 0.75 0.75]	
Jacksonville, FL	30.45	-81.6	[1 2 0.5 0.5]	SE
Kansas City, MO	39.15	-94.55	[1 2 1 1]	W, S
Knoxville, TN	35.95	-84	[0.75 1 0.75 0.75]	
Las Vegas, NV	36.2	-115.2	[1 2 1 1]	
Los Angeles, CA	34	-117.9	[1 2 1 1]	
Memphis, TN	35.1	-90.1	[1 2 0.5 0.5]	W, NW
Miami, FL	26.05	-80.3	[1 2 1 1]	
Minneapolis, MN	44.95	-93.25	[1 2 1 1]	
Montreal, QC	45.6	-73.7	[1 2 1 1]	

Nashville, TN	36.2	-86.6	[0.5 1 0.5 0.5]	
New Orleans, LA	30.05	-90.3	[1 2 1 1]	W, NW
New York, NY	40.85	-73.7	[1 2 1 1]	W, SW
Omaha, NE	41.3	-96.05	[1 2 0.5 0.5]	
Orlando, FL	28.5	-81.3	[0.5 1 0.5 0.5]	
Philadelphia, PA	40	-75.2	[1 1 0.5 0.5]	SW, NE
Phoenix, AZ	33.6	-112	[1 2 1 1]	
Pittsburgh, PA	40.4	-79.95	[1 2 1 1]	W, NW
Portland, OR	45.45	-122.55	[1 2 1 1]	
Reno, NV	39.55	-119.7	[1 2 0.5 0.5]	SW
Richmond, VA	37.4	-77.3	[0.5 1 0.5 0.5]	
Sacramento, CA	38.65	-121.4	[0.5 1 0.5 0.5]	S, SW, W
Salt Lake City, UT	40.7	-111.95	[0.75 1.5 0.75 0.75]	
San Antonio, TX	29.55	-98.45	[1 2 0.5 0.5]	NE
San Diego, CA	32.8	-117	[1 1 0.5 0.5]	
San Francisco, CA	37.6	-122	[1 2 1 1]	NE
Seattle, WA	47.35	-122.25	[1 1.5 1 1]	
St Louis, MO	38.65	-90.35	[1 2 1 1]	
Tampa, FL	27.9	-82.4	[0.75 1.5 0.75 0.75]	N, NE
Toronto, ON	43.7	-79.5	[1 2 1 1]	S, SE
Tucson, AZ	32.25	-110.85	[1 2 0.5 0.5]	NW, SE
Washington, DC	38.9	-77	[0.75 1.5 0.75 0.75]	NE, W

Table S4

Calculated *t*-scores and tabulated *t*-scores for the number of degrees of freedom in each lifetime fit for the difference between each pair of key years for the cities used in Fig. 3. For cities with increasing/decreasing lifetime, only one pair of years are shown. For cities with concave up or down lifetimes, two pairs are shown.

City	Years	t_{calc}	t_{table}	Years	t_{calc}	t_{table}
Albuquerque	2006->2010	6.49	1.99			
Atlanta	2006->2008	5.71	1.98	2008->2011	2.32	1.98
Charlotte	2008->2009	5.3	2			
Cincinnati	2010->2011	3.17	2			
Cleveland	2006->2009	7.29	2.03	2009->2010	6.11	2.03
Columbus	2008->2009	3.74	2.02			
Dallas	2006->2010	6.41	1.99	2010->2013	3.55	1.98
Denver	2006->2010	6.88	1.99	2010->2013	4.98	1.98
Indianapolis	2006->2013	8.5	2			
Jacksonville	2011->2012	3.99	1.98			
Kansas City	2006->2009	8.64	1.99	2009->2011	2.53	1.98
Knoxville	2006->2008	2.1	2	2008->2012	5.8	2.01
Los Angeles	2006->2010	2.91	1.98	2010->2013	3.29	1.98
Memphis	2006->2010	10.22	1.99	2010->2013	13.51	1.99
Minneapolis	2006->2013	10.77	1.99			
Montreal	2006->2009	5.75	1.98	2009->2013	8.09	1.99
Nashville	2006->2013	5.15	2.02			
New Orleans	2007->2009	7.99	1.99	2009->2012	8.28	1.99
New York	2006->2011	6.92	1.99	2011->2013	2.42	1.98
Omaha	2007->2013	6.92	1.99			
Orlando	2007->2009	2.43	2.01			
Philadelphia	2006->2007	3.78	2	2007->2013	3.62	2
Pittsburgh	2011->2013	10.33	1.99			
Reno	2006->2011	9.44	1.99			
San Diego	2006->2013	7.91	2.01			
San Francisco	2006->2011	2.09	1.98			
St Louis	2006->2007	4.75	1.98	2007->2013	11.15	1.99
Tampa	2006->2011	11.23	2.01			
Toronto	2008->2013	5.27	1.98			
Tucson	2009->2013	3.45	1.98			
Washington DC	2006->2009	4.7	1.99	2009->2013	9.56	2

Table S5

Rate constants used in the steady-state model.

Constant	Value
NO_2/NO	4
α	0.04
$P(HO_x)$	6.25×10^6 molec. cm^{-3} s^{-1}
k_{OH+NO2}	$k = \left(\frac{a}{1+\frac{a}{b}}\right) \cdot 0.6^p$ where $a = 1.51 \times 10^{-30} \cdot M$ $b = 2.58 \times 10^{-11}$ $p = \left[1 + \log_{10}\left(\frac{a}{b}\right)^2\right]^{-1}$
k_{RO2+NO}	8×10^{-12} cm^3 molec.$^{-1}$ s^{-1}
$k_{RO2+RO2}$	6.8×10^{-14} cm^3 molec.$^{-1}$ s^{-1}
$k_{RO2+HO2}$	8×10^{-12} cm^3 molec.$^{-1}$ s^{-1}
$k_{HO2+HO2}$	$k = 3.5 \times 10^{-13} \cdot e^{430/T} + 1.7 \times 10^{-33} \cdot (M - [H_2O]) \cdot e^{1000/T} \cdot \left[1 + 1.4 \times 10^{-21} \cdot [H_2O] \cdot e^{2200/T}\right]$ letting $[H_2O] = 0.01M$
k_{HO2+NO}	$k = 3.5 \times 10^{-12} \cdot e^{250/T}$
$k_{2,eff}$	8×10^{-12} cm^3 molec.$^{-1}$ s^{-1}
k_4	1.1×10^{-11} cm^3 molec.$^{-1}$ s^{-1}
$k_{5,eff}$	5×10^{-12} cm^3 molec.$^{-1}$ s^{-1}

References and Notes

<jrn>1. M. Wegmann, A. Fehrenbach, S. Heimann, H. Fehrenbach, H. Renz, H. Garn, U. Herz, NO_2-induced airway inflammation is associated with progressive airflow limitation and development of emphysema-like lesions in C57bl/6 mice. *Exp. Toxicol. Pathol.* **56**, 341–350 (2005). doi:10.1016/j.etp.2004.12.004 Medline</jrn>

<jrn>2. M. Kampa, E. Castanas, Human health effects of air pollution. *Environ. Pollut.* **151**, 362–367 (2008). doi:10.1016/j.envpol.2007.06.012 Medline</jrn>

<jrn>3. A. J. Haagen-Smit, E. F. Darley, M. Zaitlin, H. Hull, W. Noble, Investigation on injury to plants from air pollution in the Los Angeles area. *Plant Physiol.* **27**, 18–34 (1952). doi:10.1104/pp.27.1.18 Medline</jrn>

<jrn>4. S. N. Pandis, R. A. Harley, G. R. Cass, J. H. Seinfeld, Secondary organic aerosol formation and transport. *Atmos. Environ. A* **26**, 2269–2282 (1992). doi:10.1016/0960-1686(92)90358-R</jrn>

<jrn>5. C. A. Pope 3rd, M. Ezzati, D. W. Dockery, Fine-Particulate Air Pollution and Life Expectancy in the United States, Fine-particulate air pollution and life expectancy in the United States. *N. Engl. J. Med.* **360**, 376–386 (2009). doi:10.1056/NEJMsa0805646 Medline</jrn>

<jrn>6. R. Burnett, H. Chen, M. Szyszkowicz, N. Fann, B. Hubbell, C. A. Pope 3rd, J. S. Apte, M. Brauer, A. Cohen, S. Weichenthal, J. Coggins, Q. Di, B. Brunekreef, J. Frostad, S. S. Lim, H. Kan, K. D. Walker, G. D. Thurston, R. B. Hayes, C. C. Lim, M. C. Turner, M. Jerrett, D. Krewski, S. M. Gapstur, W. R. Diver, B. Ostro, D. Goldberg, D. L. Crouse, R. V. Martin, P. Peters, L. Pinault, M. Tjepkema, A. van Donkelaar, P. J. Villeneuve, A. B. Miller, P. Yin, M. Zhou, L. Wang, N. A. H. Janssen, M. Marra, R. W. Atkinson, H. Tsang, T. Quoc Thach, J. B. Cannon, R. T. Allen, J. E. Hart, F. Laden, G. Cesaroni, F. Forastiere, G. Weinmayr, A. Jaensch, G. Nagel, H. Concin, J. V. Spadaro, Global estimates of mortality associated with long-term exposure to outdoor fine particulate matter. *Proc. Natl. Acad. Sci. U.S.A.* **115**, 9592–9597 (2018). doi:10.1073/pnas.1803222115 Medline</jrn>

<bok>7. G. Myhre, D. Shindle, F.-M. Bréon, W. Collins, J. Fuglestvedt, J. Huang, D. Koch, J.-F. Lamarque, D. Lee, B. Mendoza, T. Nakajima, A. Robock, G. Stephens, T. Takemura, H. Zhang, *Climate Change 2013: The Physical Science Basis. Contribution of Working Group I to the Fifth Assessment Report of the Intergovernmental Panel on Climate Change* (Cambridge Univ. Press, 2013), pp. 659–740.</bok>

<jrn>8. L. C. Valin, A. R. Russell, R. C. Cohen, Variations of OH radical in an urban plume inferred from NO_2 column measurements. *Geophys. Res. Lett.* **40**, 1856–1860 (2013). doi:10.1002/grl.50267</jrn>

<jrn>9. E. C. Browne, P. J. Wooldridge, K.-E. Min, R. C. Cohen, On the role of monoterpene chemistry in the remote continental boundary layer. *Atmos. Chem. Phys.* **14**, 1225–1238 (2014). doi:10.5194/acp-14-1225-2014</jrn>

<jrn>10. S. Beirle, K. F. Boersma, U. Platt, M. G. Lawrence, T. Wagner, Megacity emissions and lifetimes of nitrogen oxides probed from space. *Science* **333**, 1737–1739 (2011). doi:10.1126/science.1207824 Medline</jrn>

<jrn>11. F. Liu, S. Beirle, Q. Zhang, S. Dörner, K. He, T. Wagner, NO_x lifetimes and emissions of cities and power plants in polluted background estimated by satellite observations. *Atmos. Chem. Phys.* **16**, 5283–5298 (2016). doi:10.5194/acp-16-5283-2016</jrn>

<jrn>12. J. L. Laughner, Q. Zhu, R. C. Cohen, The Berkeley high resolution tropospheric NO_2 product. *Earth Syst. Sci. Data* **10**, 2069–2095 (2018). doi:10.5194/essd-10-2069-2018</jrn>

<bok>13. J. Laughner, Q. Zhu, R. Cohen, Berkeley High Resolution (BEHR) OMI NO2–Native pixels, daily profiles, v5, UC Berkeley Dash, Dataset (2018); doi:10.6078/D1WH41 </bok>

<jrn>14. J. L. Laughner, A. Zare, R. C. Cohen, Effects of daily meteorology on the interpretation of space-based remote sensing of NO_2. *Atmos. Chem. Phys.* **16**, 15247–15264 (2016). doi:10.5194/acp-16-15247-2016</jrn>

<jrn>15. J. G. Murphy, D. A. Day, P. A. Cleary, P. J. Wooldridge, D. B. Millet, A. H. Goldstein, R. C. Cohen, The weekend effect within and downwind of Sacramento—Part 1: Observations of ozone, nitrogen oxides, and VOC reactivity. *Atmos. Chem. Phys.* **7**, 5327–5339 (2007). doi:10.5194/acp-7-5327-2007</jrn>

<jrn>16. L. C. Marr, R. A. Harley, Modeling the Effect of Weekday-Weekend Differences in Motor Vehicle Emissions on Photochemical Air Pollution in Central California, Modeling the effect of weekday-weekend differences in motor vehicle emissions on photochemical air pollution in central California. *Environ. Sci. Technol.* **36**, 4099–4106 (2002). doi:10.1021/es020629x Medline</jrn>

<foot>17. Materials and methods are available as supplementary materials.</foot>

<jrn>18. Z. Lu, D. G. Streets, B. de Foy, L. N. Lamsal, B. N. Duncan, J. Xing, Emissions of nitrogen oxides from US urban areas: Estimation from Ozone Monitoring Instrument retrievals for 2005–2014. *Atmos. Chem. Phys.* **15**, 10367–10383 (2015). doi:10.5194/acp-15-10367-2015</jrn>

<jrn>19. F. Liu, S. Beirle, Q. Zhang, R. J. van der A, B. Zheng, D. Tong, K. He, NO_x emission trends over Chinese cities estimated from OMI observations during 2005 to 2015. *Atmos. Chem. Phys.* **17**, 9261–9275 (2017). doi:10.5194/acp-17-9261-2017 Medline</jrn>

<jrn>20. Z. Jiang, B. C. McDonald, H. Worden, J. R. Worden, K. Miyazaki, Z. Qu, D. K. Henze, D. B. A. Jones, A. F. Arellano, E. V. Fischer, L. Zhu, K. F. Boersma, Unexpected slowdown of US pollutant emission reduction in the past decade. *Proc. Natl. Acad. Sci. U.S.A.* **115**, 5099–5104 (2018). doi:10.1073/pnas.1801191115 Medline</jrn>

<jrn>21. S. E. Pusede, A. L. Steiner, R. C. Cohen, Temperature and recent trends in the chemistry of continental surface ozone. *Chem. Rev.* **115**, 3898–3918 (2015). doi:10.1021/cr5006815 Medline</jrn>

<jrn>22. R. F. Silvern, D. J. Jacob, L. J. Mickley, M. P. Sulprizio, K. R. Travis, E. A. Marais, R. C. Cohen, J. L. Laughner, S. Choi, J. Joiner, L. N. Lamsal, Using satellite observations of tropospheric NO_2 columns to infer long-term trends in US NO_x emissions: The importance of accounting for the free tropospheric NO_2 background. *Atmos. Chem. Phys. Discuss.* **2019**, 1–26 (2019). doi:10.5194/acp-2019-168</jrn>

<other>23. J. L. Laughner, behr-github/NAm-NOx-Lifetime: version 1.3 (2019); doi:10.5281/zenodo.3386680.</other>

<other>24. J. L. Laughner, R. C. Cohen, Supporting data for “Direct observation of changing NO_x lifetime in North American cities” (2019); doi:10.6078/D1RQ4V.</other>

<jrn>25. J. L. Laughner, Q. Zhu, R. Cohen, Evaluation of version 3.0B of the BEHR OMI NO_2 product. *Atmos. Meas. Tech.* **12**, 129–146 (2019). doi:10.5194/amt-12-129-2019</jrn>

<bok>26. A. Krotkov Nickolay, P. Veefkind, *OMI/Aura Nitrogen Dioxide (NO2) Total and Tropospheric Column 1-orbit L2 Swath 13x24 km V003, Greenbelt, MD, USA, Goddard Earth Sciences Data and Information Services Center (GES Dros. Inf. Serv.C)* (2016).</bok>

<bok>27. C. Z. W. Schaaf, *MCD43D07 MODros. Inf. Serv./Terra+Aqua BRDF/Albedo Parameter1 Band3 Daily L3 Global 30ArcSec CMG V006. NASA EOSDros. Inf. Serv. Land Processes DAAC* (2015); https://doi.org/10.5067/modis/mcd43d07.006.</bok>

<bok>28. C. Z. W. Schaaf, *MCD43D08 MODros. Inf. Serv./Terra+Aqua BRDF/Albedo Parameter2 Band3 Daily L3 Global 30ArcSec CMG V006. NASA EOSDros. Inf. Serv. Land Processes DAAC* (2015); https://doi.org/10.5067/modis/mcd43d08.006.</bok>

<bok>29. C. Z. W. Schaaf, *MCD43D09 MODros. Inf. Serv./Terra+Aqua BRDF/Albedo Parameter3 Band3 Daily L3 Global 30ArcSec CMG V006. NASA EOSDros. Inf. Serv. Land Processes DAAC* (2015); https://doi.org/10.5067/modis/mcd43d09.006.</bok>

<bok>30. C. Z. W. Schaaf, *MCD43D31 MODros. Inf. Serv./Terra+Aqua BRDF/Albedo QA BRDFQuality Daily L3 Global 30ArcSec CMG V006. NASA EOSDros. Inf. Serv. Land Processes DAAC* (2015); https://doi.org/10.5067/modis/mcd43d31.006.</bok>

<bok>31. D. A. Hastings, P. K. Dunbar, *Global Land One-Kilometer Base Elevation (GLOBE) Digital Elevation Model, Documentation, Volume 1.0. Key to Geophysical Records Documentation (KGRD) 34* (National Oceanic and Atmospheric Administration, 1999).</bok>

<jrn>32. A. R. Russell, L. C. Valin, R. C. Cohen, Trends in OMI NO_2 observations over the United States: Effects of emission control technology and the economic recession. *Atmos. Chem. Phys.* **12**, 12197–12209 (2012). doi:10.5194/acp-12-12197-2012</jrn>

<eref>33. Research Data Archive at the National Center for Atmospheric Research, I. S. Laboratory, *NCEP North American Regional Reanalysis (NARR)* (Boulder CO, 2005); http://rda.ucar.edu/datasets/ds608.0.</eref>

<jrn>34. V. G. Dovì, O. Paladino, A. P. Reverberi, Some remarks on the use of the inverse Hessian matrix of the likelihood function in the estimation of statistical properties of parameters. *Appl. Math. Lett.* **4**, 87–90 (1991). doi:10.1016/0893-9659(91)90129-J</jrn>

<jrn>35. P. A. Jiménez, J. Dudhia, Improving the representation of resolved and unresolved topographic effects on surface wind in the WRF model. *J. Appl. Meteorol. Climatol.* **51**, 300–316 (2012). doi:10.1175/JAMC-D-11-084.1</jrn>

<bok>36. D. C. Harris, *Quantitative Chemical Analysis* (W.H. Freeman, ed. 8, 2010), pp. 76–78.</bok>

<other>37. J. L. Laughner, *PECANS (Python Editable Chemical Atmospheric Numeric Solver)* Zenodo (2019); doi:10.5281/zenodo.3386652.</other>

<jrn>38. M. B. Dillon, M. S. Lamanna, G. W. Schade, A. H. Goldstein, R. C. Cohen, Chemical evolution of the Sacramento urban plume: Transport and oxidation. *J. Geophys. Res. Atmos.* **107** (D5), ACH 3-1, ACH 3-15 (2002). doi:10.1029/2001JD000969</jrn>

<jrn>39. N. A. Krotkov, L. N. Lamsal, E. A. Celarier, W. H. Swartz, S. V. Marchenko, E. J. Bucsela, K. L. Chan, M. Wenig, M. Zara, The version 3 OMI NO_2 standard product. *Atmos. Meas. Tech.* **10**, 3133–3149 (2017). doi:10.5194/amt-10-3133-2017</jrn>

<jrn>40. J. G. Murphy, D. A. Day, P. A. Cleary, P. J. Wooldridge, D. B. Millet, A. H. Goldstein, R. C. Cohen, The weekend effect within and downwind of Sacramento: Part 2. Observational evidence for chemical and dynamical contributions. *Atmos. Chem. Phys. Discuss.* **6**, 11971–12019 (2006). doi:10.5194/acpd-6-11971-2006</jrn>